PHYSICAL REVIEW A **94**, 031603(R) (2016)

# Predicted scaling behavior of Bloch oscillation in Weyl semimetals

Yan-Qi Wang and Xiong-Jun Liu*
*International Center for Quantum Materials, School of Physics, Peking University, Beijing 100871, China*
*and Collaborative Innovation Center of Quantum Matter, Beijing 100871, China*
(Received 29 May 2016; published 20 September 2016)

We predict a fundamental scaling law of Bloch oscillation in Weyl semimetals, which manifests that the transverse drift of quasiparticles accelerated bypassing a Weyl point exhibits asymptotically a linear log-log relation with respect to the minimal momentum measured from the Weyl point. This scaling relation is deeply connected to the topological monopole structure of Weyl points, thus being universal and providing a scheme to measure bulk topology of Weyl semimetals.

DOI: 10.1103/PhysRevA.94.031603

*Introduction.* Weyl semimetals (WSMs), being a new type of free fermion topological states [1–5], have attracted fast growing attention since the experimental discovery in the solid state material TaAs last year [6–8]. Differently from topological insulators, which have gap in the bulk and gapless modes in the boundary [9,10], WSMs exhibit gapless bulk nodal points, called Weyl points, with the low-energy quasiparticles known as Weyl fermions. A Weyl point is topologically protected, and has definite chirality which is characterized by Chern number defined on two-dimensional (2D) gapless Fermi surface enclosing the node and figured as magnetic monopole in momentum space [11,12]. In a WSM the following fundamental question can be of particular interest: What is the unique physical observable which can characterize the gapless Weyl fermions and topological monopole structure at Weyl points? So far a number of fascinating physics have been predicted for WSMs, including surface Fermi arc states [1–3] and different magnetotransport anomalies [4,12–19], with some of them having been observed in recent experiments [6–8]. Nevertheless, those effects are not uniquely related to the topological monopoles at Weyl points, thus providing indirect rather than direct measurements of the bulk topology of WSMs.

Recently, fueled by the great progress in experiments, the synthetic spin-orbit (SO) coupling [20–24] and gauge fields [25–27] have developed into a most active area for cold atoms [28–30]. In the presence of synthetic SO coupling or gauge fields, many novel topological states have been proposed and studied [31–39], including the three-dimensional (3D) Weyl semimetals in optical lattices [40,41]. Compared with solid state materials, cold atoms offer advantages to detecting topological states, e.g., through direct measurement of the bulk states which can hardly be observed for solids [42–46]. These studies motivate us to explore new fundamental physics of WSMs which can uniquely characterize Weyl fermions and topological monopoles at Weyl points, with which the experimental scheme of observing bulk topology of WSMs shall be proposed.

In this Rapid Communication, we predict a linear logarithmical scaling law of Bloch oscillation dynamics in WSMs and propose to detect the Weyl nodal points based on this universal behavior. Being a consequence of the topological monopole structure nearby Weyl points, the transverse drift of quasiparticles accelerated bypassing a Weyl point is shown to exhibit a linear log-log relation with respect to the minimal momentum from the Weyl point. The monopole Berry curvature, chirality, and anisotropy of the Weyl point can be read out from the predicted scaling law. Applications of the predicted scaling to realistic optical lattice models of WSMs are considered, with which we demonstrate the feasibility of identifying topological Weyl nodal points in experiment.

*Continuous model.* We start with a continuous model for generic WSMs of type I or II [47–50]. The continuous Hamiltonian nearby a Weyl point reads (taking $\hbar = 1$)

$$\mathcal{H}(\mathbf{k}) = \mathbf{v_0 k_x} \otimes \mathbf{1} + \sum_{\mathbf{j=x,y,z}} \mathbf{v_j k_j} \sigma_{\mathbf{j}}, \tag{1}$$

where $\mathbf{1}$ is a $2 \times 2$ unit matrix, the coefficients $v_0$ and $v_j$ ($j = x,y,x$) determine the velocity of quasiparticles along the $j$ direction, and $\sigma_{x,y,z}$ are Pauli matrices. For $v_0 \neq 0$, the velocity of quasiparticles is symmetric in both $y$ and $z$ directions, but asymmetric in the $x$ direction. In particular, when $|v_0| > |v_x|$, the $x$ component of the velocity is always positive (for $v_0 > 0$) or negative (for $v_0 < 0$), rendering a type II WSM [47–50]. The Berry connection $\mathcal{A}_-(\mathbf{k}) = i \langle u_{-,\mathbf{k}} | \nabla_{\mathbf{k}} | u_{-,\mathbf{k}} \rangle$, with $|u_{-,\mathbf{k}}\rangle$ the eigenstates for the lower subband. The Berry curvature $\vec{\mathcal{B}}_-(\mathbf{k}) = \nabla_{\mathbf{k}} \times \mathcal{A}_-(\mathbf{k}) = v_x v_y v_z \mathbf{k}/[2(\sum_j v_j^2 k_j^2)^{3/2}]$, showing a magnetic monopole located at $\mathbf{k} = \mathbf{0}$. The topology of the Weyl point is characterized by the first Chern number, which is calculated by the integral of Berry curvature throughout a surface enclosing the Weyl point at $\mathbf{k} = \mathbf{0}$, namely, $C_{\mathbf{1}} = \frac{1}{2\pi} \oint d\mathbf{S} \cdot \vec{\mathcal{B}}_-(\mathbf{k})$. Direct calculations give $C_{\mathbf{1}} = 1$, reflecting the chirality of the Weyl point.

We study Bloch dynamics of a quasiparticle at the lower subband, by applying an external force $\vec{F}$ [44]. The semiclassical dynamics is governed by $\dot{k}_j = F_j$, $\dot{r}_j = \partial_{k_j} \mathcal{E}_-(\mathbf{k}) - \epsilon_{jkl} F_k \mathcal{B}_l^-$, where $\mathcal{E}_\pm(\mathbf{k}) = v_0 k_x \pm (\sum_j v_j^2 k_j^2)^{1/2}$ with $\mathbf{r}$ and $\mathbf{k}$ the center-of-mass position and momentum, respectively. The transverse drift induced by monopole Berry curvature $\vec{\mathbf{S}} = -\int \vec{F} \times \vec{\mathcal{B}}_-(\mathbf{k}) dt = -\int d\mathbf{k} \times \vec{\mathcal{B}}_-(\mathbf{k})$, which is independent of force strength but sensitive to magnitude of Berry curvature. The transverse drifts induced by two Weyl points with opposite chiralities are in the opposite directions, providing a simple measurement of the chirality of a Weyl point. Without loss of generality, we set the initial momentum as $\mathbf{k_0} = \mathbf{k_0 \hat{e}_n} =$

*Corresponding author: xiongjunliu@pku.edu.cn

 

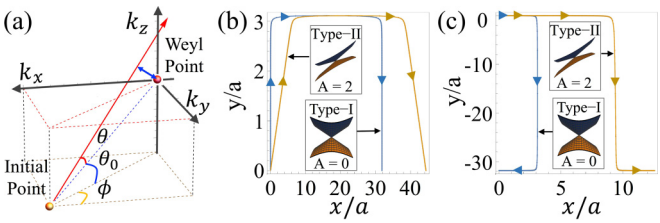


FIG. 1. (a) Parameters in continuous model. The red and blue arrows stand for $\vec{F}$ direction and $k_{\min}$, respectively. (b), (c) Trajectory of BEC cloud for type I and type II WSMs. Transverse drift occurs, respectively, in the $x$ direction with parameters $\mathbf{k_0} = -\mathbf{k_0}\hat{\mathbf{e}}_\mathbf{y}$, $\mathbf{F_x} = \mathbf{0}$, $\mathbf{F_y} = \mathbf{F}\cos\theta$, and $F_z = -F\sin\theta$ (b), and in the $y$ direction with parameters $\mathbf{k_0} = -\mathbf{k_0}\hat{\mathbf{e}}_\mathbf{x}$, $\mathbf{F_x} = \mathbf{F}\cos\theta$, $\mathbf{F_y} = \mathbf{0}$, and $F_z = -F\sin\theta$ (c).

$\mathbf{k_0}\cos\theta_0\cos\phi\hat{\mathbf{e}}_\mathbf{x} + \mathbf{k_0}\cos\theta_0\sin\phi\hat{\mathbf{e}}_\mathbf{y} - \mathbf{k_0}\sin\theta_0\hat{\mathbf{e}}_\mathbf{z}$, where $\hat{e}_n$ is a unit vector, and $\theta_0 + \pi/2$ and $\phi$ are, respectively, its polar and azimuthal angles in the spherical coordinate constructed on the Weyl point, as shown in Fig. 1(a). A generic force is then described by $\vec{F} = -F\cos(\theta_0+\theta)\cos\phi\hat{e}_x - F\cos(\theta_0+\theta)\sin\phi\hat{e}_y + F\sin(\theta_0+\theta)\hat{e}_z$, with $\theta$ being the angle between $\vec{F}$ and $-\mathbf{k_0}$. The transverse drift, after a long enough time evolution, is integrated out via $S[t\to\infty] = |\int_0^\infty \vec{F}\times\vec{\mathcal{B}}_-(\mathbf{k})dt|$, giving

$$S[t\to\infty] = \frac{v_x v_y\left[\sqrt{\sum_i(\hat{e}_n\cdot\hat{e}_i)^2 v_i^2} + P(\theta)\right]}{v_z k_0\sin\theta\left(v_x^2\cos^2\phi + v_y^2\sin^2\phi\right)}, \tag{2}$$

where $P(\theta) \equiv [(v_x^2\cos^2\phi + v_y^2\sin^2\phi)\{[\cos\theta_0 + \cos(\theta_0+\theta)]\cos(\theta_0+\theta) - 2\cos(\theta_0)^2\} + v_z^2\{[\sin(\theta_0+\theta) + \sin\theta_0]\sin(\theta_0+\theta) - 2\sin^2(\theta_0)\}][4\sum_i(\hat{e}_n\cdot\hat{e}_i)^2 v_i^2]^{-1/2}$. In the small angle limit $\theta\to 0$, we have $P(\theta)\to 0$ and $k_{\min}S = v_x v_y\sqrt{\sum_i(\hat{e}_n\cdot\hat{e}_i)^2 v_i^2}/v_z(v_x^2\cos^2\phi + v_y^2\sin^2\phi)$, with $k_{\min}\equiv|k_0\sin\theta|$ the minimal momentum measured from the Weyl point in the whole dynamical process. With this result, we reach a linear log-log scaling

$$\ln S = -\ln k_{\min} + \ln\frac{v_x v_y\sqrt{\sum_i(\hat{e}_n\cdot\hat{e}_i)^2 v_i^2}}{v_z\left(v_x^2\cos^2\phi + v_y^2\sin^2\phi\right)}, \quad \theta\to 0. \tag{3}$$

This relation is deeply rooted in the fact that in the small $\theta$ limit, $S$ is dominated by the monopole Berry curvature close to the Weyl point, which exhibits the inverse square law $|\vec{\mathcal{B}}(\mathbf{k})| \propto 1/k^2$. Thus this log-log scaling behavior is universal and model independent, as we shall further prove in the lattice models. The intercept of $\ln S$ in Eq. (3) reflects the anisotropy of the Weyl point, and vanishes if the Weyl point is isotropic ($v_x = v_y = v_z$), for arbitrary $\theta_0$ and $\phi$. In particular, when $\theta_0 = 0$ and $\phi = -\pi/2$ (i.e., $\mathbf{k_0} = -\mathbf{k_0}\hat{\mathbf{e}}_\mathbf{y}$), the intercept is $D_x = \ln(v_x/v_z)$, which measures the anisotropy of the Weyl point with respect to the two ($x$ and $z$) directions perpendicular to the applied force. Similarly, we have $D_{y(z)} = \ln(v_{y(z)}/v_{x(y)})$ for $\mathbf{k_0} = -\mathbf{k_0}\hat{\mathbf{e}}_{\mathbf{z(x)}}$. Therefore, by measuring the scaling and the intercepts we can read out the complete information of a Weyl point. It is interesting that the above scaling behavior is valid for both type I and type II WSMs, while the two different types of WSMs can be distinguished in experiments by the trajectories of quasiparticles accelerated bypassing the Weyl point, as shown in Figs. 1(b) and 1(c) [51].

*Scaling law in lattice models.* We proceed to study the scaling in lattice models for cold atoms. In experiment the Bloch dynamics can be performed for a Bose-Einstein condensate (BEC) prepared at the band bottom. Such BEC cloud can be described by a wave packet with a typical radius of several sites. Unlike in a continuous model, in optical lattices the BEC exhibits periodic motion along the applied force, while the transverse drift shall be accumulated during the Bloch oscillation involving certain Weyl points [51]. In the following calculation we consider that the noninteracting BEC evolves from the band bottom and passes by a certain Weyl point only one time before ending at some final state, so the information of such Weyl point can be extracted out. Two typical lattice models for WSMs shall be considered by generating synthetic gauge fields and SO coupling.

The first spinless model for our investigation was proposed by Dubček *et al.*, who studied a Weyl semimetal in a cubic lattice, formed by two ($A$ and $B$) sublattices, by generating synthetic gauge potentials via laser-assisted tunneling (LAT) [40]. The Bloch Hamiltonian in their realization takes the form

$$\begin{aligned}\mathcal{H}(\mathbf{k}) = &-2J_y\cos(k_y a)\tau_x - 2K_x\sin(k_x a)\tau_y \\ &+ 2K_z\cos(k_z a)\tau_z,\end{aligned} \tag{4}$$

where the Pauli matrices $\tau_{x,y,z}$ act on the pseudospin (sublattice) space, $(K_x, J_y)$ denote the amplitudes of tunneling between $A$ and $B$ sites, and $K_z$ represents the $AA$ and $BB$ hopping along the $z$ direction [40]. The lattice constant can be set as $a = 1$ to facilitate further discussions.

The Hamiltonian (4) preserves time-reversal (TR) symmetry defined as $\mathcal{T} = \mathcal{K}$, with $\mathcal{K}$ being the complex conjugate for spinless system. With the TR symmetry, the system has four independent Weyl points at $\{\mathbf{k_w}\} = (\mathbf{0}, \pm\pi/\mathbf{2}, \pm\pi/\mathbf{2})$, nearby which the Hamiltonian is linearized as $\mathcal{H}(\mathbf{k}) = -2K_x k_x\tau_y \pm 2J_y k_y\tau_x \pm 2K_z k_z\tau_z$. The magnitude of Berry curvature is shown in Fig. 2(b).

The band bottom is located at four different Bloch momenta $\{\mathbf{k_0}\} = \{(\pm\pi/\mathbf{2},\mathbf{0},\mathbf{0}),(\pm\pi/\mathbf{2},\mathbf{0},\pi)\}$. Let the BEC cloud be prepared at $\mathbf{k_0} = (-\pi/\mathbf{2},\mathbf{0},\mathbf{0})$ and then accelerated by an external force toward one of the four Weyl points. For this purpose the force can be applied in the $\hat{e}_\pm$-$\hat{e}_y$ plane, with $\hat{e}_\pm = (\hat{e}_x \pm \hat{e}_z)/\sqrt{2}$. Specifically, one has $F_x = (F/\sqrt{2})\cos(\theta_0+\theta)$, $F_z = \pm(F/\sqrt{2})\cos(\theta_0+\theta)$, and $F_y = \pm F\sin(\theta_0+\theta)$ with $\theta_0 = \arcsin\sqrt{1/3}$. When $\theta = 0$ the force points from $\mathbf{k_0}$ to one of the four Weyl points. Under this configuration and in the limit $\theta\to 0$, the linear scaling [51] is $\ln S = -\ln k_{\min} + D_{\rm LAT}$, with the intercept

$$D_{\rm LAT} = \frac{1}{2}\ln\left[\frac{1}{3}\left(1 + 2\frac{K^2}{J_y^2}\right)\right]. \tag{5}$$

Here the two LAT couplings $K_x$ and $K_z$ have been set as $K_x = K_z = K$ [40]. Numerical results are shown in Fig. 2(c). It can be seen that when the lattice is isotropic in all three directions, i.e., $J_y = K$, the intercept vanishes (red curves), whereas a nonzero intercept appears for the linear scaling line when the Weyl points are anisotropic. Moreover, from Fig. 2(c) one can find that the relation between $S$ and $k_{\min}$ approaches

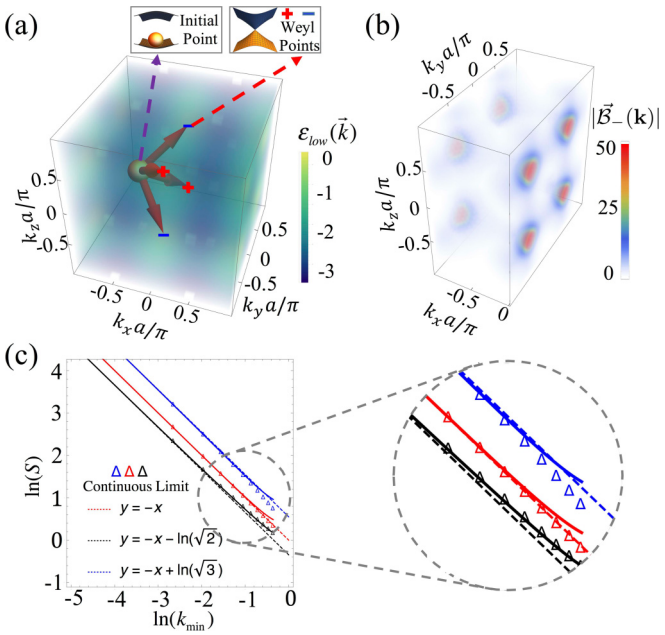


FIG. 2. WSM realized with LAT scheme. (a) Schematic diagram for BEC cloud accelerated from initial momentum toward Weyl points. (b) Magnitude of Berry curvature. The parameters are taken as with $J_y = K_z = K_x = 1.0$, $|\vec{\mathcal{B}}_-(\mathbf{k})|$ over 50 is plotted in red. (c) Scaling relation between drift $S$ and $k_{\min}$, with parameters $2J_y = K_z = K_x$ (upper, blue lines), $J_y = K_z = K_x$ (middle, red lines), and $0.5J_y = K_z = K_x$ (lower, black lines). The triangle, solid, and dotted lines represent results based on the low-energy continuous Hamiltonian, on the full lattice Hamiltonian, and asymptotic scaling lines given by Eq. (3), respectively. All parameters are rescaled to be dimensionless.

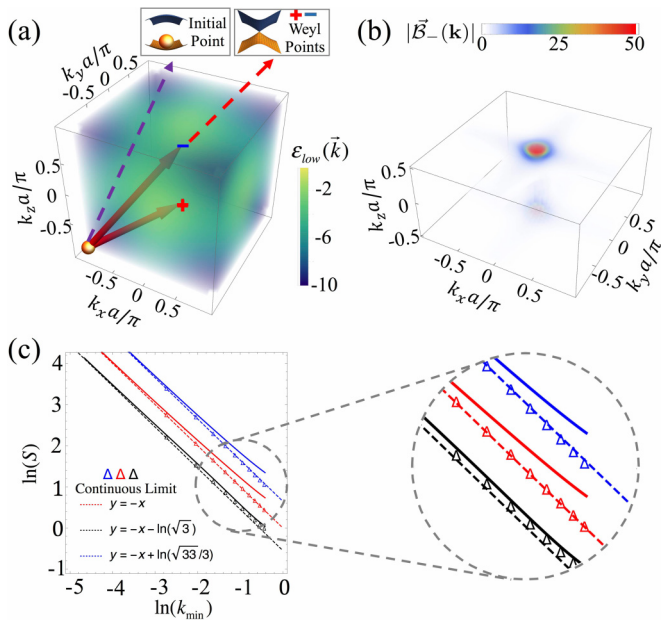


FIG. 3. WSM realized with SO coupled lattice. (a) Sketch for BEC cloud accelerated from initial momentum to Weyl points. (b) Magnitude of Berry curvature. The parameters $t_{\rm SO} = t_z = 1.1t_0$, $m_z = 4t_0$, $|\vec{\mathcal{B}}_-(\mathbf{k})|$ over 50 is plotted in red. (c) Scaling with parameters $t_z = 0.5t_{\rm SO}$ (upper, blue lines), $t_z = t_{\rm SO}$ (middle, red lines), and $t_z = 2t_{\rm SO}$ (lower, black lines). The triangle, solid, and dotted lines represent results based on the low-energy continuous Hamiltonian, on the full lattice Hamiltonian, and asymptotic scaling lines, respectively.

quickly the linear log-log relation when $k_{\min}$ is less than 0.1, consistent with the analytic result of the continuous model in Eq. (3). It is expected that the Weyl points can be well detected in the realistic cold atom experiments.

Now we turn to the study of the scaling relation in a SO coupled WSM, which can be realized by generalizing the 2D SO coupling scheme [35] to 3D cubic lattice system [51]. Note that this 2D SO coupling for Bose condensates has been realized in a recent experiment [52]. We propose a 3D tight-binding Hamiltonian for the WSM as

$$\begin{aligned} H = &-\sum_{\langle\vec{i},\vec{j}\rangle} t_\alpha(\hat{c}^\dagger_{\vec{i}\uparrow}\hat{c}_{\vec{j}\uparrow} - \hat{c}^\dagger_{\vec{i}\downarrow}\hat{c}_{\vec{j}\downarrow}) + \sum_{\vec{i}} m_z(\hat{n}_{\vec{i}\uparrow} - \hat{n}_{\vec{i}\downarrow}) \\ &+ \left[\sum_{j_x} t_{\rm so}\left(\hat{c}^\dagger_{j_x\uparrow}\hat{c}_{j_x+1\downarrow} - \hat{c}^\dagger_{j_x\uparrow}\hat{c}_{j_x-1\downarrow}\right) + \text{H.c.}\right] \\ &+ \left[\sum_{j_y} i t_{\rm SO}\left(\hat{c}^\dagger_{j_y\uparrow}\hat{c}_{j_y+1\downarrow} - \hat{c}^\dagger_{j_y\uparrow}\hat{c}_{j_y-1\downarrow}\right) + \text{H.c.}\right]. \quad (6) \end{aligned}$$

Here $t_{\alpha=x,y,z}$ and $t_{\rm so}$ denotes, respectively, the spin-conserved and spin-flip hopping, and $m_z$ represents an effective Zeeman term [35]. Transforming $H$ into the momentum space yields $H = \sum_{k,\sigma,\sigma'} \hat{c}^\dagger_{\mathbf{k},\sigma}\mathcal{H}_{\sigma,\sigma'}(k)\hat{c}_{\mathbf{k},\sigma'}$, with $\mathcal{H}(k) = 2t_{\rm so}\sin(k_y)\sigma_x + 2t_{\rm so}\sin(k_x)\sigma_y + (m_z - 2t_x\cos k_x - 2t_y\cos k_y - 2t_z\cos k_z)\sigma_z$.

For convenience, we assume that the lattice is isotropic in the $x$ and $y$ directions, i.e., $t_x = t_y = t_0$. Here the TR symmetry $\mathcal{T} = i\sigma_y\mathcal{K}$ is broken. In the case with $2|2t_0 - t_z| \leqslant m_z \leqslant 2(2t_0 + t_z)$ and $m_z \geqslant 2t_z$ (for $t_0, t_z > 0$), the above Hamiltonian has only two Weyl points located in the $z$ axis. In particular, for $m_z = 4t_0$ the two Weyl points are $\mathbf{k_{w(1,2)}} = (\mathbf{0},\mathbf{0},\pm\frac{\pi}{2})$, with the Weyl cone Hamiltonian

$$\mathcal{H}_\pm(k) = 2t_{\rm SO}(k_y\sigma_x + k_x\sigma_y) + (t_0k_\perp^2 \pm 2t_zk_z)\sigma_z, \quad (7)$$

where $k_\perp^2 \equiv k_x^2 + k_y^2$. The monopole Berry curvature nearby the Weyl points is shown in Fig. 3(b).

The band bottom of the system is located at $\mathbf{k_0} = (-\pi,-\pi,-\pi)$ [Fig. 3(a)], where the BEC cloud can be accelerated toward one of the two Weyl points by a force with $\phi = \pi/4$ and $\theta_0 = \arcsin(1/3)$ in Fig. 1(a). In the limit $\theta \to 0$ the atomic cloud is towards the Weyl point $(0,0,-\pi/2)$. The intercept of the linear scaling reads

$$D_{\rm SO} = \frac{1}{2}\ln\left|\frac{1}{9} + \frac{8t_{\rm SO}^2}{9t_z^2}\right|. \quad (8)$$

We present the numerical results in Fig. 3(c), which show some features different from those in the previous LAT model. First, the intercept vanishes for $t_{\rm SO} = t_z$ and it is independent of the hopping $t_0$ in the $x$ and $y$ directions. Second, due to the quadratic momentum term ($\propto k_\perp^2$), which is the leading correction to the Weyl cone Hamiltonian (7) and absent in LAT model, the relation between $S$ and $k_{\min}$ approaches the linear log-log relation slowly. Nevertheless, we can see that this linear scaling relation can be well reflected when $k_{\min} < 0.05$.

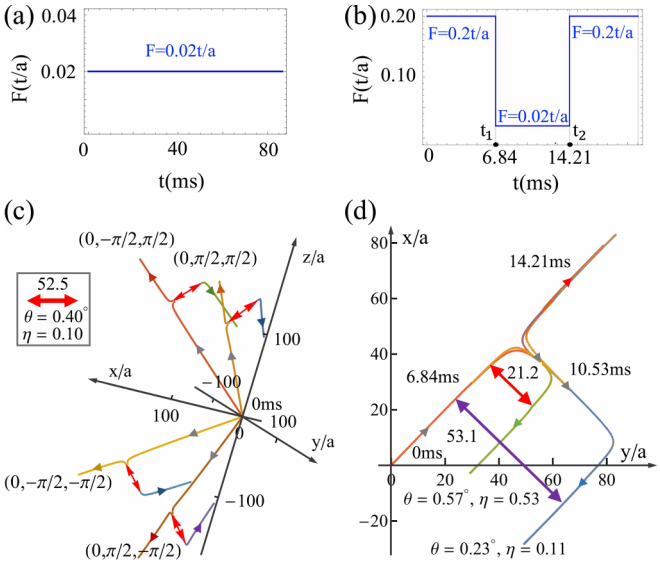


FIG. 4. (a), (b) Manipulation of external force for WSMs in LAT model (a) and SO coupled model (b). (c) Trajectory of BEC cloud to four Weyl points in LAT model, with $K_x = K_z = J_y = t = 2\pi \times 0.5$ kHz. (d) Trajectory of BEC cloud in SO coupled model, projected onto the $x$-$y$ plane, with $t_{SO} = t_z = t = 2\pi \times 0.52$ kHz $= 1.1t_0$ and $m_0 = 4t_0$. Double arrows in (c) and (d) denote the transverse drifts.

*Landau-Zener transition.* When the BEC cloud is accelerated close to the Weyl point, the Landau-Zener (LZ) transition of the atoms occurs from the lower to higher subbands [53,54]. To ensure a sufficiently high resolution in experiments, one requires that the remaining BEC cloud in the lower subband after LZ transition, quantified by $\eta = 1 - P_{LZ}$, should not be too small. Here $P_{LZ} = \exp(-\frac{\pi E_{min}^2}{4Fv_f})$ is the transition probability, with $v_f$ the velocity of the Weyl cone along the force direction and $E_{min}$ the energy difference between particle and hole states at the avoided crossing during the Bloch oscillation [53,54]. To measure the scaling behavior, we need to properly tune the force and its direction ($\theta$). First, a small angle $\theta$ (small $k_{min}$) is necessary to ensure that the relation between the transverse drift $S$ and $k_{min}$ enters the linear regime. Second, a finite ratio of the BEC cloud is left in the lower subband after LZ transition so that the remaining atom cloud can be imaged. For fixed $k_{min}$, though a small external force can supress LZ transition, it however leads to a large Bloch oscillation period which should not exceed the BEC lifetime.

For the WSM realized with LAT scheme, which has relatively long lifetime, we apply a small constant force to observe the scaling law, as shown in Figs. 4 (a) and 4(c). The numerical results show that more than $\eta = 10\%$ of the BEC cloud remains in the lower subband after the atom cloud passes by the Weyl point, with the angle $\theta = 0.4^\circ$ or $k_{min} \approx 0.02$, which is well within the linear scaling regime according to Fig. 2(c). On the other hand, for the SO coupled lattice model, to satisfy the aforementioned requirements, we introduce a timing sequence to manipulate the external force. When $0 < t < t_1 = 6.84$ ms and $t > t_2 = 14.21$ ms, a relatively strong force of magnitude $F_1 = 0.2t/a$ is applied, while within $t_1 < t < t_2$, when the BEC cloud evolves very close to the Weyl point, a weak force of magnitude $F_2 = 0.02t/a$ is applied [Fig. 4(b)]. With this manipulation we find the remaining BEC cloud after LZ transition to be $\eta = 1 - P_{LZ} = [1 - \exp(-\frac{\pi E(t_1)^2}{4F_1 v_f(t_1)})][1 - \exp(-\frac{\pi E_{min}^2}{4F_2 v_f})]$ [51]. Here $E(t_1)$ and $v_f(t_1)$ stand for the energy difference between particle and hole states and the velocity at $t = t_1$, respectively. From the numerical results in Fig. 4(d) we find that for an angle no less than $\theta = 0.23^\circ$, which corresponds to $k_{min} = 0.02$, the ratio of the remaining BEC cloud is over 10% in the typical parameter regimes. Thus the linear scaling law is observable with this configuration. Note that the atoms populated in the upper subband after LZ transition move back along the traverse direction and eventually their transverse drift cancels since Berry curvature is opposite for the lower and upper subbands [Figs. 4(c) and 4(d)]. Thus the transverse drift of the BEC cloud in the lower subband can be experimentally determined by the distance between the two split BEC clouds after LZ transition along the transverse direction [51].

*Conclusion.* We have predicted a linear logarithmical scaling law of Bloch oscillation in WSMs and proposed that the scaling behavior can be applied to detect topological Weyl points. The transverse drift of quasiparticles accelerated bypassing a Weyl point is shown to exhibit asymptotically a linear log-log relation with respect to the minimal momentum measured from the Weyl point. Being deeply connected to the topological monopole structure nearby Weyl points, this scaling relation manifests a universal dynamical response to external force and can be used to characterize Weyl fermions. Thus the predicted scaling provides a novel measurement of the complete information of topological Weyl nodes, with the feasibility having been demonstrated by considering two typical models of WSMs realized in optical lattices. These results will push forward new experimental studies of WSMs, particularly in cold atoms.

*Acknowledgments.* We thank Colin J. Kennedy, Long Zhang, and Bao-Zong Wang for helpful discussions. This work is supported by MOST (Grant No. 2016YFA0301600), NSFC (Grant No. 11574008), President's Fund for Undergraduate Research of Peking University, and Thousand-Young-Talent Program of China.

[1] X. Wan, A. M. Turner, A. Vishwanath, and S. Y. Savrasov, Phys. Rev. B **83**, 205101 (2011).

[2] G. Xu, H. Weng, Z. Wang, X. Dai, and Z. Fang, Phys. Rev. Lett. **107**, 186806 (2011).

[3] A. A. Burkov and L. Balents, Phys. Rev. Lett. **107**, 127205 (2011).

[4] P. Hosur, S. A. Parameswaran, and A. Vishwanath, Phys. Rev. Lett. **108**, 046602 (2012).

[5] J.-H. Jiang, Phys. Rev. A **85**, 033640 (2012).

[6] S.-Y. Xu *et al.*, Science **349**, 613 (2015).

[7] B. Q. Lv, H. M. Weng, B. B. Fu, X. P. Wang, H. Miao, J. Ma, P. Richard, X. C. Huang, L. X. Zhao, G. F. Chen, Z.

Fang, X. Dai, T. Qian, and H. Ding, Phys. Rev. X **5**, 031013 (2015).
[8] X. Huang, L. Zhao, Y. Long, P. Wang, D. Chen, Z. Yang, H. Liang, M. Xue, H. Weng, Z. Fang, X. Dai, and G. Chen, Phys. Rev. X **5**, 031023 (2015).
[9] M. Z. Hasan and C. L. Kane, Rev. Mod. Phys. **82**, 3045 (2010).
[10] X.-L. Qi and S.-C. Zhang, Rev. Mod. Phys. **83**, 1057 (2011).
[11] H. B. Nielsen and M. Ninomiya, Nucl. Phys. B **185**, 20 (1981).
[12] H. B. Nielsen and M. Ninomiya, Phys. Lett. B **130**, 389 (1983).
[13] A. A. Zyuzin and A. A. Burkov, Phys. Rev. B **86**, 115133 (2012).
[14] D. T. Son and B. Z. Spivak, Phys. Rev. B **88**, 104412 (2013).
[15] S. A. Parameswaran, T. Grover, D. A. Abanin, D. A. Pesin, and A. Vishwanath, Phys. Rev. X **4**, 031035 (2014).
[16] Q.-D. Jiang, H. Jiang, H. Liu, Q.-F. Sun, and X. C. Xie, Phys. Rev. Lett. **115**, 156602 (2015).
[17] C. Zhang *et al.*, arXiv:1503.02630v1.
[18] J. Xiong, S. K. Kushwaha, T. Liang, J. W. Krizan, W. Wang, R. Cava, and N. Ong, arXiv:1503.08179v1.
[19] S. A. Yang, H. Pan, and F. Zhang, Phys. Rev. Lett. **115**, 156603 (2015).
[20] X.-J. Liu, M. F. Borunda, X. Liu, and J. Sinova, Phys. Rev. Lett. **102**, 046402 (2009).
[21] Y.-J. Lin, K. Jiménez-García, and I. B. Spielman, Nature (London) **471**, 83 (2011).
[22] J.-Y. Zhang, S.-C. Ji, Z. Chen, L. Zhang, Z.-D. Du, B. Yan, G.-S. Pan, B. Zhao, Y.-J. Deng, H. Zhai, S. Chen, and J.-W. Pan, Phys. Rev. Lett. **109**, 115301 (2012).
[23] P. Wang, Z.-Q. Yu, Z. Fu, J. Miao, L. Huang, S. Chai, H. Zhai, and J. Zhang, Phys. Rev. Lett. **109**, 095301 (2012).
[24] L. W. Cheuk, A. T. Sommer, Z. Hadzibabic, T. Yefsah, W. S. Bakr, and M. W. Zwierlein, Phys. Rev. Lett. **109**, 095302 (2012).
[25] M. Aidelsburger, M. Atala, M. Lohse, J. T. Barreiro, B. Paredes, and I. Bloch, Phys. Rev. Lett. **111**, 185301 (2013).
[26] H. Miyake, G. A. Siviloglou, C. J. Kennedy, W. C. Burton, and W. Ketterle, Phys. Rev. Lett. **111**, 185302 (2013).
[27] M. Aidelsburger *et al.*, Nat. Phys. **11**, 162 (2015).
[28] N. Goldman, G. Juzeliūnas, P. Öhberg, and I. B. Spielman, Rep. Prog. Phys. **77**, 126401 (2014).
[29] X. Zhou, Y. Li, Z. Cai, and C. Wu, J. Phys. B: At., Mol. Opt. Phys. **46**, 134001 (2013).
[30] H. Zhai, Rep. Prog. Phys. **78**, 026001 (2015).
[31] X.-J. Liu, X. Liu, C. Wu, and J. Sinova, Phys. Rev. A **81**, 033622 (2010).
[32] N. Goldman, J. Beugnon, and F. Gerbier, Phys. Rev. Lett. **108**, 255303 (2012).
[33] X.-J. Liu, Z.-X. Liu, and M. Cheng, Phys. Rev. Lett. **110**, 076401 (2013).
[34] X. Li, E. Zhao, and W. V. Liu, Nat. Commun. **4**, 1523 (2013).
[35] X.-J. Liu, K. T. Law, and T. K. Ng, Phys. Rev. Lett. **112**, 086401 (2014); **113**, 059901 (2014).
[36] S.-T. Wang, D.-L. Deng, and L.-M. Duan, Phys. Rev. Lett. **113**, 033002 (2014).
[37] Y. Xu and C. Zhang, Phys. Rev. Lett. **114**, 110401 (2015).
[38] C. Hickey, L. Cincio, Z. Papić, and A. Paramekanti, Phys. Rev. Lett. **116**, 137202 (2016).
[39] H. Chen, X.-J. Liu, and X. C. Xie, Phys. Rev. Lett. **116**, 046401 (2016).
[40] T. Dubček, C. J. Kennedy, L. Lu, W. Ketterle, M. Soljačić, and H. Buljan, Phys. Rev. Lett. **114**, 225301 (2015).
[41] W.-Y. He, S. Zhang, and K. T. Law, Phys. Rev. A **94**, 013606 (2016).
[42] E. Alba, X. Fernandez-Gonzalvo, J. Mur-Petit, J. K. Pachos, and J. J. García-Ripoll, Phys. Rev. Lett. **107**, 235301 (2011).
[43] H. M. Price and N. R. Cooper, Phys. Rev. A **85**, 033620 (2012).
[44] X.-J. Liu, K. T. Law, T. K. Ng, and P. A. Lee, Phys. Rev. Lett. **111**, 120402 (2013).
[45] D.-L. Deng, S.-T. Wang, and L.-M. Duan, Phys. Rev. A **90**, 041601(R) (2014).
[46] X.-J. Liu, Z.-X. Liu, K. T. Law, W. V. Liu, and T. K. Ng, New J. Phys. **18**, 035004 (2016).
[47] A. A. Soluyanov, D. Gresch, Z. Wang, Q. Wu, M. Troyer, X. Dai, and B. A. Bernevig, Nature (London) **527**, 495 (2015).
[48] E. J. Bergholtz, Z. Liu, M. Trescher, R. Moessner, and M. Udagawa, Phys. Rev. Lett. **114**, 016806 (2015); M. Trescher, B. Sbierski, P. W. Brouwer, and E. J. Bergholtz, Phys. Rev. B **91**, 115135 (2015).
[49] Y. Xu, F. Zhang, and C. Zhang, Phys. Rev. Lett. **115**, 265304 (2015).
[50] J. Jiang *et al.*, arXiv:1604.00139v1.
[51] See Supplemental Material at http://link.aps.org/supplemental/10.1103/PhysRevA.94.031603 for more details of transverse drift, Bloch oscillation, and Landau-Zener transition.
[52] Z. Wu *et al.*, arXiv:1511.08170v1.
[53] C. Zener, Proc. R. Soc. London, Ser. A **137**, 696 (1932).
[54] L. D. Landau, Phys. Z. **2**, 46 (1932).